

the  $\gamma$  counter and the  $\alpha$ -particle counter, the Doppler shift of the photons<sup>18</sup> is

$$\frac{\Delta E_\gamma}{E_\gamma} = -\frac{v'}{c} \cos\theta' + \frac{v_{\text{c.m.}}}{c} \cos\varphi, \quad (2)$$

where  $v'$  is the velocity of the  $\text{C}^{12}$  nucleus in the center-of-mass system and  $v_{\text{c.m.}}$  is the center-of-mass velocity. For convenience, we regard the  $\gamma$  counter as a point counter. Then the photons of nominal energy  $E$  in coincidence with  $\alpha$  particles will have a range of energy

$$d(\Delta E) = E(v'/c) \sin\theta' d\theta'.$$

Here  $d\theta'$  is the mean angular aperture of the  $\alpha$  counter in the plane defined by the  $\alpha$ -particle and photon directions, and is related to the center-of-mass angular aperture,  $\delta'$ , of our (circular)  $\alpha$  counter by  $d\theta' = 2a\delta'$ , where the coefficient  $a$  depends on  $\varphi$  and the center-of-mass transformation. We then note that an  $\alpha$  particle

<sup>18</sup> Effects proportional to  $v^2/c^2$  are negligible.

emitted anywhere in the cone of half-angle  $\theta'$  can be associated with a photon of the correct energy incident on the  $\gamma$  counter. The coincidence counting rate,  $N_c$ , must thus be corrected by the factor  $2\pi \sin\theta' (2\delta'/\Omega_\alpha')$ , where  $\Omega_\alpha'$  is the solid angle of the  $\alpha$  counter. The number of photons per unit energy interval is thus

$$N(E) = \frac{N_c}{E(v'/c) \sin\theta' d\theta'} \left( \frac{(2\pi \sin\theta') 2\delta'}{\Omega_\alpha'} \right) = \frac{1}{a} \left( \frac{2\pi N_c}{(v'/c) E \Omega_\alpha'} \right).$$

For the scattering experiment, we wish to know how this compares with the average value of  $N(E)$  over the whole line, i.e., with  $\langle N(E) \rangle_{\text{Av}} = N_\gamma c / (2Ev')$ ,  $N_\gamma$  being the singles  $\gamma$  rate in the coincidence experiment. Dividing by the average value, we find

$$\frac{N(E)}{\langle N(E) \rangle_{\text{Av}}} = \frac{4\pi}{a} \left( \frac{N_c}{\Omega_\alpha' N_\gamma} \right). \quad (3)$$

## Back-Angle Elastic Scattering of 14.6-Mev Neutrons\*

J. D. ANDERSON, C. C. GARDNER, M. P. NAKADA, AND C. WONG  
*University of California Radiation Laboratory, Livermore Site, Livermore, California*  
 (Received December 4, 1957)

Differential elastic scattering cross sections have been obtained for 14.6-Mev neutrons on Fe, Ag, Cd, Sn, and Pb in 5° steps from 90° to 167°. Time-of-flight techniques and one-meter radius rings were used to reduce background, obtain reasonable counting rates, and preserve angular resolution. Optical model calculations by Bjorklund and Fernbach indicate that a spin-orbit coupling term is needed to fit the data.

### I. INTRODUCTION

PREVIOUSLY published measurements of elastic scattering angular distributions for 14-Mev neutrons have not extended beyond 90°.<sup>1</sup> Excellent fits to these data have been obtained through optical model calculations in spite of the different potentials and parameters used.<sup>2-4</sup> In the region beyond 90°, however, the predictions of the various models are quite different. By making measurements beyond 90°, it was hoped that the choice of potentials and parameters could be narrowed; in addition, the prediction<sup>2</sup> of deep minima at back angles could be checked.

Large-angle measurements with 14-Mev neutrons

\* Work was performed under the auspices of the U. S. Atomic Energy Commission.

<sup>1</sup> J. H. Coon *et al.*, *Bull. Am. Phys. Soc. Ser. II*, **2**, 233, 1957 (reports measurements to 140°).

<sup>2</sup> Bjorklund, Fernbach, and Sherman, *Phys. Rev.* **101**, 1832 (1956).

<sup>3</sup> Beyster, Walt, and Salmi, *Phys. Rev.* **104**, 1319 (1956).

<sup>4</sup> W. S. Emmerich, Westinghouse Research Laboratories, Research Report 60-94511-6-R 17, 1957 (unpublished).

have been difficult because of low signal and high background levels. To overcome these difficulties, a pulsed-beam time-of-flight<sup>5</sup> method with large ring geometry was adopted. The elastically scattered neutrons were then effectively time-separated from a large part of the background neutrons and gamma rays. Since gamma rays produced by the neutrons in the scatterer were also time-separated from elastically scattered neutrons, a large and efficient detector could be used.

### II. EXPERIMENTAL DETAILS

#### Geometry

The experimental geometry is shown in Fig. 1. The 500-keV deuteron beam from the Cockcroft-Walton accelerator is swept and bunched<sup>6</sup> before striking a tritium-loaded titanium target. Two-milli-

<sup>5</sup> L. Cranberg and J. S. Levin, *Phys. Rev.* **103**, 343 (1956).

<sup>6</sup> Ashby, Harris, Klein, and Nakada, University of California Radiation Laboratory Report UCRL-4641, 1955 (unpublished).

microsecond bursts of neutrons are emitted nearly isotropically with a mean energy of 14.6 Mev at  $45^\circ$ . A 1-meter radius scattering ring is placed at  $45^\circ$  to the deuteron beam direction, the plane of the ring is perpendicular to the beam line. Neutrons scattered from the ring are detected in a plastic scintillator located on the ring axis. An absorber placed between the target and detector attenuates the direct neutrons.

The scattering angle was varied by moving the detector along the ring axis. For measurements between  $90^\circ$  and  $155^\circ$ , a 20-inch copper absorber was used. The measurements were extended to  $167^\circ$  by use of a 10-inch tungsten absorber. Neutrons transmitted through the absorber are time-separated from the elastically scattered neutrons; the difference in flight paths yields a time separation of 40 millimicroseconds at  $167^\circ$  and 16 millimicroseconds at  $90^\circ$ .

### Electronics

A schematic diagram of the electronics is shown in Fig. 2. The pulses in the plastic scintillator were

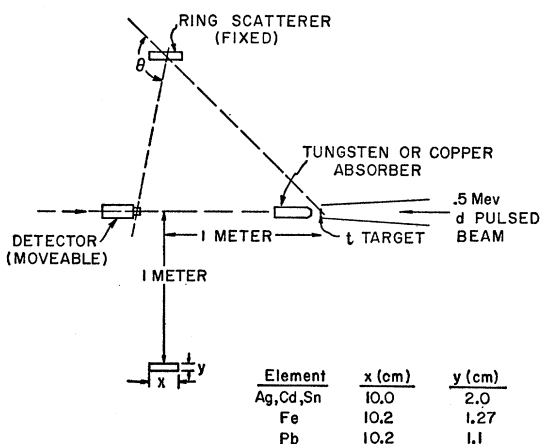


Fig. 1. Schematic drawing of the experimental geometry. Scattering angle is denoted by  $\theta$ .

viewed by an RCA 6342 photomultiplier. The anode signal of the photomultiplier passes through a cathode follower, linear amplifier, and into a discriminator gate unit. This relatively slow and stable channel sets the bias level. The fast channel consists of the output of the last dynode of the photomultiplier amplified by Hewlett Packard wide-band amplifiers and fed directly into the start channel of the "time-to-pulse height converter."<sup>7</sup> Pulses produced by the arrival of the deuteron bursts on the target are delayed 0.16 microsecond and amplified by wide-band amplifiers before entering the stop channel of the converter. The output of the converter is amplified and fed into an Argonne type 256-channel pulse-height analyzer, which is gated by the output of the discriminator gate.

<sup>7</sup> Weber, Johnstone, and Cranberg, Rev. Sci. Instr. 27, 166 (1956).

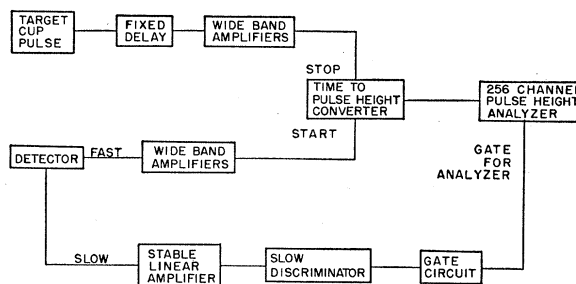


Fig. 2. Schematic diagram of the electronics.

### Detector Calibration

The relative production of neutrons was monitored by counting the alpha particles from the  $T(dn)He^4$  reaction in a proportional counter. A  $BF_3$  long counter was used as an auxiliary monitor.

The detector bias was set by observing the proton recoils occurring in the plastic scintillator. For this purpose the detector was set at about  $98^\circ$  to the deuteron beam direction, since neutrons emitted at this angle are the most monoenergetic. Since at  $98^\circ$  the neutron energy is 14.0-Mev, the recoil spectrum determines the 14-Mev bias setting. Bias settings below 14-Mev were deduced by using the proton pulse-height-versus-energy curves for a plastic scintillator.<sup>8</sup> Neutron detector biases of 12.1 and 10.8 Mev were employed. For both biases the over-all time resolution of the electronics and the deuteron burst width as measured by the full width at half-maximum of the direct neutrons was about 3 millimicroseconds (Fig. 3).

After setting the slow-channel bias, the efficiency of the detector was measured by having it sample neutrons identical to those incident on the scattering ring. The detector was calibrated before and after a signal run; the two efficiencies agreed within statistics indicating

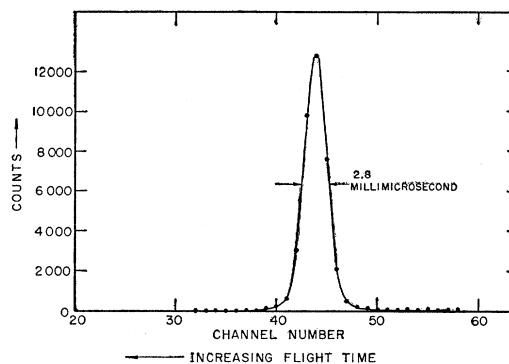


Fig. 3. Time spectrum with detector viewing neutrons emitted at  $45^\circ$  to the tritium target. As indicated, the resolution of the time-of-flight equipment is 2.8 millimicroseconds. The sum of the counts under the peak yields the detector efficiency for 14.6-Mev neutrons. Time scale of the analyzer is set at 1 millimicrosecond/channel.

<sup>8</sup> Ball, Booth, and MacGregor (private communication).

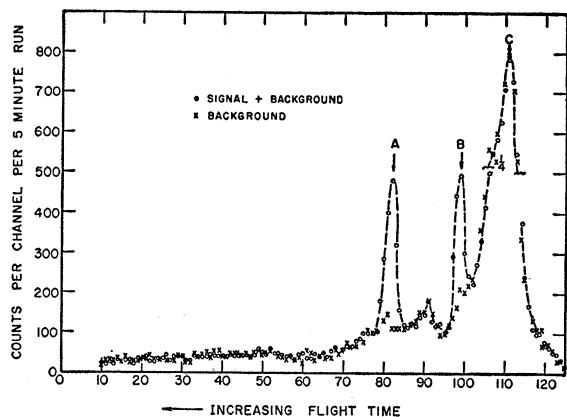


FIG. 4. Typical time spectra for iron signal and background at  $\theta=140^\circ$ . *A* denotes neutrons elastically scattered from iron; *B* denotes gamma rays following inelastic scattering of neutrons from iron; *C* denotes neutrons transmitted through absorber. Time separation between elastics and gammas is 17 millimicroseconds and between elastics and directs is 29 millimicroseconds.

electronic stability. A typical efficiency time spectrum is shown in Fig. 3.

### III. RESULTS

Typical time spectra for the signal and background are shown in Fig. 4. For each element background runs were taken either immediately before or after the signal run to minimize the effect of any drifts. The elastic scattering counts were obtained by plotting the signal and background and making the appropriate subtractions (Fig. 5). The differential elastic scattering cross sections were obtained by the following formula:

$$\sigma(\theta) = \frac{(\text{elastic counts})}{(\text{calib. counts})^*} \left( \frac{R_0}{X} \right)^2 \frac{A}{R^2} \frac{1}{M} \frac{1}{0.602 \text{ steradian}}, \text{ barns}$$

where  $(\text{calib. counts})^* =$  calibration counts for a neutron production equivalent to that of scattering runs,

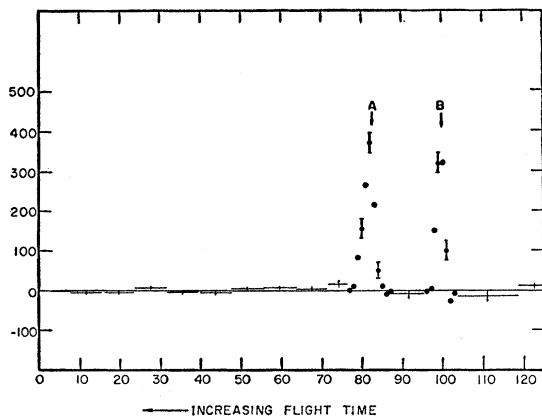


FIG. 5. Signal minus background for iron at  $\theta=140^\circ$ . *A* denotes neutrons elastically scattered from iron, while *B* denotes gamma rays following inelastic scattering of neutrons from iron.

$R_0$ =distance from target to ring,  $X$ =distance from target to calibration position,  $R$ =distance from ring to detector,  $A$ =atomic weight, and  $M$ =mass of ring.

Corrections for absorption, multiple scattering, and angular resolution were calculated with a Monte Carlo code on the UNIVAC. The angular resolution correction does not include the finite detector size. This results in an angular spread of less than  $\pm 2^\circ$ .

The efficiency inserted into the formula is that for 14.6-Mev neutrons (neutrons scattered through  $0^\circ$ ). For other scattering angles the neutrons suffer elastic energy degradation, and hence the efficiency is reduced relative to the zero-degree scattering efficiency. The

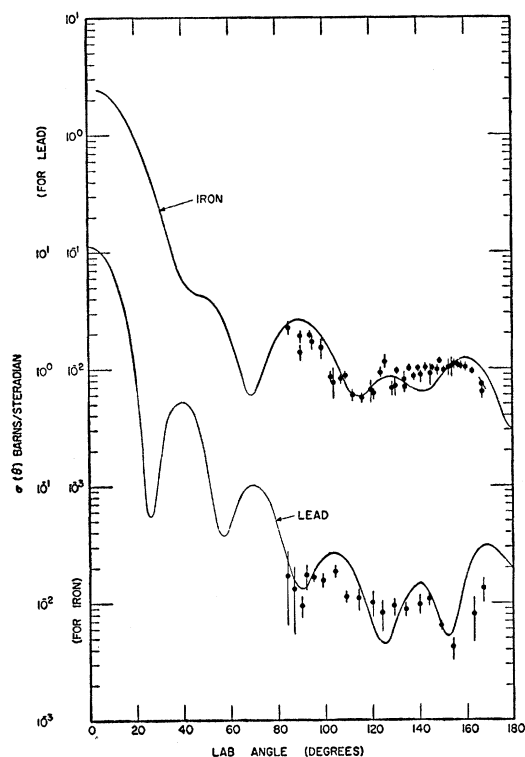


FIG. 6. Measured angular distributions for Fe and Pb. The solid curves are the predictions of Bjorklund and Fernbach employing a spin-orbit coupling term.

correction for this effect was computed by assuming the efficiency of the detector to be proportional to  $\sigma(E-E_b)/E$ , where  $E_b$  is the energy equivalent of the detector bias,  $E$  is the incident neutron energy, and  $\sigma$  is the  $n-p$  cross section at energy  $E$ . The cross sections corrected for all the above effects are plotted in Figs. 6-7.

### IV. ERRORS

The sources of error can be divided into two categories: those affecting the relative shape of the angular distribution and those affecting the general level of the distribution. The relative errors consist of counting statistics, accuracy of background subtrac-

tions, and uncertainty in the efficiency correction due to an uncertainty in determining the bias energy. The absolute errors consist of the uncertainties in the efficiency determination and uncertainties in the absorption and multiple-scattering corrections. For each element the above errors were estimated and then combined under the assumption that they were statistically independent.

An additional uncertainty which affects both of the above categories is the contribution from inelastically scattered neutrons. The fact that 12.1- and 10.8-Mev bias measurements yield the same cross sections within statistics indicates that there is no appreciable contribution from inelastic neutrons.

### V. CONCLUSIONS

With the exception of lead, the experimental data do not show the deep minima at back angles predicted by optical models without spin-orbit coupling.<sup>2</sup> The predictions of Bjorklund and Fernbach<sup>9</sup> employing a spin-orbit term are shown plotted in Figs. 6 and 7 (solid curve). Comparison with the experimental points shows that there is quantitative as well as qualitative agreement. The theoretical predictions also fit the existing scattering data for angles less than 90°.<sup>9</sup>

### ACKNOWLEDGMENTS

The authors are indebted to S. Fernbach and F. Bjorklund for many discussions concerning their optical model, to M. Mansigh and J. Hudson for

<sup>9</sup> F. E. Bjorklund and S. Fernbach, University of California Radiation Laboratory Report UCRL-4932 (unpublished).

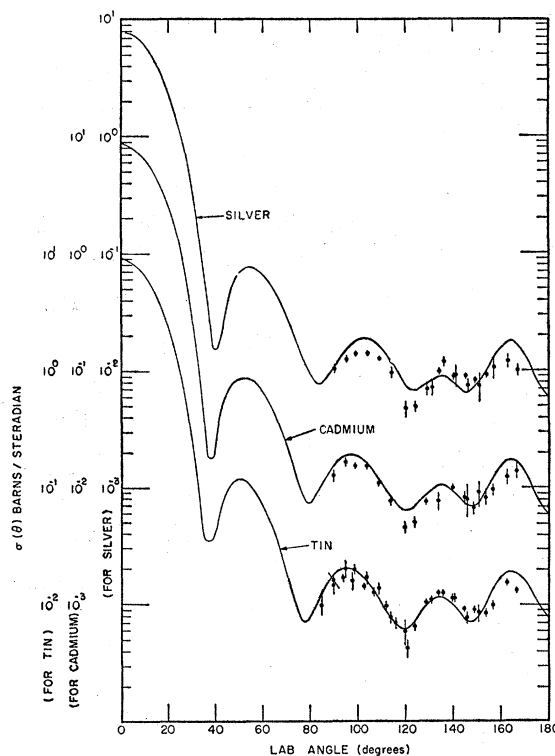


FIG. 7. Measured angular distributions for Ag, Cd, and Sn. The solid curves are the predictions of Bjorklund and Fernbach employing a spin-orbit coupling term.

programming and running the Monte Carlo calculations, and to J. M. Peterson for continued encouragement during the course of the experiment.

## Proton Polarization Measurements near 18 Mev\*

KARL W. BROCKMAN, JR.†

Palmer Physical Laboratory, Princeton University, Princeton, New Jersey

(Received December 3, 1957)

Polarization of protons in proton-helium scattering may be calculated from phase shifts obtained from differential cross section measurements. Calculations of this type were performed for energies up to 18 Mev. On the basis of these results, an instrument was built with which proton polarizations could be measured for protons with energies from 5 Mev to 18 Mev and beyond. A second polarization analyzer was built utilizing the discovery of polarization in the scattering of protons by carbon around 17 Mev. Results are given for polarization measurements on H, D, Be, C, and Al near 18 Mev. Angular distributions for polarization in both elastic and inelastic (4.4-Mev excitation) scattering by carbon are also reported.

### I. INTRODUCTION

WHILE polarization of protons by nuclear scattering at energies in excess of 100 Mev has received a great deal of attention during the past several years,<sup>1</sup>

\* Supported by the U. S. Atomic Energy Commission and the Higgins Scientific Trust Fund.

† Now at Institute for Nuclear Studies, Amsterdam, Netherlands.

<sup>1</sup> A comprehensive bibliography of pre-1956 polarization papers may be found in L. Wolfenstein's review article, *Annual Reviews*

there has been relatively little interest in the possibility of obtaining polarizations at lower energies. It was, in fact, thought that such polarization should not exist; the high-energy polarization appeared to decrease with energy in such a way that it could be expected to vanish around bombarding energies of 50 Mev.<sup>2</sup> Recent

of *Nuclear Science* (Annual Reviews, Inc., Stanford, 1956), Vol. 6, p. 43.

<sup>2</sup> J. Marshall (private communication, 1955).